Chemical Science

ROYAL SOCIETY OF CHEMISTRY

EDGE ARTICLE

View Article Online
View Journal | View Issue

Cite this: *Chem. Sci.*, 2020, **11**, 3345

All publication charges for this article have been paid for by the Royal Society of Chemistry

The crucial roles of guest water in a biocompatible coordination network in the catalytic ring-opening polymerization of cyclic esters: a new mechanistic perspective†

Sheng-Chun Chen,[a] Fei-Hang Zhang,[a] Kun-Lin Huang,[b] Feng Tian,[a] Zhi-Hui Zhang,[a] Renxian Zhou,[c] Xue-Jun Feng,[a] Xiaoying Zhou,[a] Ming-Yang He,[a] Jiande Gu,*[d] Qun Chen*[a] and Chuan-De Wu*[c]

The ring-opening polymerization (ROP) of cyclic esters/carbonates is a crucial approach for the synthesis of biocompatible and biodegradable polyesters. Even though numerous efficient ROP catalysts have been well established, their toxicity heavily limits the biomedical applications of polyester products. To solve the toxicity issues relating to ROP catalysts, we report herein a biocompatible coordination network, CZU-1, consisting of $Zn_4(\mu_4\text{-}O)(COO)_6$ secondary building units (SBUs), biomedicine-relevant organic linkers and guest water, which demonstrates high potential for use in the catalytic ROP synthesis of biomedicine-applicable polyesters. Both experimental and computational results reveal that the guest water in CZU-1 plays crucial roles in the activation of the $Zn_4(\mu_4\text{-}O)(COO)_6$ SBUs by generating μ_4-OH Brønsted acid centers and Zn–OH Lewis acid centers, having a synergistic effect on the catalytic ROP of cyclic esters. Different to the mechanism reported in the literature, we propose a new reaction pathway for the catalytic ROP reaction, which has been confirmed using density functional theory (DFT) calculations, *in situ* diffuse reflectance IR Fourier transform spectroscopy (DRIFTS), and matrix-assisted laser desorption/ionization time-of-flight mass spectroscopy (MALDI-TOF MS). Additionally, the hydroxyl end groups allow the polyester products to be easily post-modified with different functional moieties to tune their properties for practical applications. We particularly expect that the proposed catalytic ROP mechanism and the developed catalyst design principle will be generally applicable for the controlled synthesis of biomedicine-applicable polymeric materials.

Received 27th November 2019
Accepted 26th February 2020

DOI: 10.1039/c9sc06024c

rsc.li/chemical-science

Introduction

The ring-opening polymerization (ROP) of cyclic esters/carbonates is a crucial approach for synthesizing biodegradable polyesters.[1] As they have been developed for more than 65 years, numerous efficient ROP catalysts have been reported in the literature,[2] including tin(II)-bis(2-ethylhexanoate),[3] aluminum alkoxides,[4] $Ln(OR)_3$ (Ln = La and Y; R = *i*-Pr and *n*-Bu),[5] and the oxo-metal alkoxides $M_5(\mu_5\text{-}O)(OR)_{13}$ (M = Fe, Y, La, Sm and Yb; R = Et and Pr).[6] However, the toxicity of these catalysts has heavily limited the biomedical applications of the produced polyesters. Therefore, developing efficient biocompatible ROP catalysts remains a crucial and essential issue for the manufacture of biomedicine-applicable polyesters.[7]

One of the key elements involved in the development of efficient ROP catalysts is understanding the catalytic mechanism of ROP reactions both experimentally[8] and theoretically.[9] Dittrich and Schulz first proposed a three-step coordination–insertion mechanism catalyzed using metal-alkoxide complexes (Scheme 1).[10] Density functional theory (DFT) calculations based on Al-alkoxide- and Sn-alkoxide-catalyzed ROP reactions showed that the three-step coordination–insertion mechanism is kinetically applicable.[11] However, there are many experimental phenomena that could not be reasonably explained using the three-step ROP mechanism, such as the important roles played by protic agents

[a]*Jiangsu Key Laboratory of Advanced Catalytic Materials and Technology, School of Petrochemical Engineering, Changzhou University, Changzhou 213164, P. R. China. E-mail: chenqunjpu@yahoo.com*

[b]*College of Chemistry, Chongqing Normal University, Chongqing 401331, P. R. China*

[c]*Department of Chemistry, Zhejiang University, Hangzhou 310027, P. R. China. E-mail: cdwu@zju.edu.cn*

[d]*Drug Design & Discovery Center, State Key Laboratory of Drug Research, Shanghai Institute of Materia Medica, CAS, Shanghai 201203, P. R. China. E-mail: jiandegu@simm.ac.cn*

† Electronic supplementary information (ESI) available: Experimental details relating to synthesis and characterization; PXRD patterns; $^1H/^{13}C$ NMR spectra; TGA curves; IR, elemental analysis, HRMS, XPS, ICP-MS, *in situ* DRIFTS, GPC, and MALDI-TOF MS data; X-ray structure determination information; cytotoxicity assays; DFT calculations; and catalytic test results. CCDC 1842876. For ESI and crystallographic data in CIF or other electronic format see DOI: 10.1039/c9sc06024c

(*e.g.*, water and alcohols) in ROP reactions. Therefore, unveiling the ROP reaction mechanism is of significant importance for the development of efficient ROP catalysts.

Metal–organic frameworks (MOFs) are a class of emerging porous materials that are constructed from coordination bond connections between metal ions/clusters and organic linkers.[12] MOFs built from oxo-metal clusters, *e.g.*, $M_3O(COO)_6$ in MIL-101 and MIL-100 (M = Fe, Cr and Al);[13] $Zn_4O(COO)_6$ in the IRMOF series[14] and UMCM-1;[15] $Zr_6O_4(OH)_4(COO)_{12}$ in the UiO series;[16] and others,[17] with coordinatively unsaturated metal sites have been used as highly efficient Lewis acid catalysts in numerous organic transformations. The catalytic efficiency can be highly improved if synergistic Brønsted acid/base sites are present in the organic linkers.[18] Since discrete oxo-metal complexes are highly active in catalyzing ROP reactions, MOFs consisting of oxo-metal cluster secondary building units (SBUs) might also be highly active in ROP reactions. Therefore, the toxicity issues relating to polyesters could be solved by developing biocompatible MOFs as ROP catalysts, such as through choosing biocompatible metal ions (*e.g.*, Zn^{II}, Fe^{III}, Zr^{IV}, Ca^{II} and Mg^{II}) and organic linkers (*e.g.*, naturally or medically relevant molecules) as building units. Herein, we report a biocompatible coordination network, $\{[Zn_4(\mu_4\text{-}O)(tzmb)_3]\cdot 0.5H_2O\}_n$ (CZU-1), built from $Zn_4(\mu_4\text{-}O)(COO)_6$ SBUs and the aromatase inhibitor letrozole derivative 4,4′-(1*H*-1,2,4-triazol-1-yl)methylene-bis(benzoate) (tzmb), which demonstrates high catalytic efficiency in the solvent-free ROP of cyclic esters for the production of biocompatible polyesters. DFT calculation results indicate that the guest water molecules in CZU-1 play crucial roles in the activation of the $Zn_4(\mu_4\text{-}O)(COO)_6$ SBUs through generating active Brønsted acid μ_4-OH and Lewis acid Zn(II)–OH sites (Scheme 2). We found that the ROP reaction pathway is different to the three-step coordination–insertion mechanism given in the literature, thus providing new insights for the development of efficient biocompatible ROP catalysts.

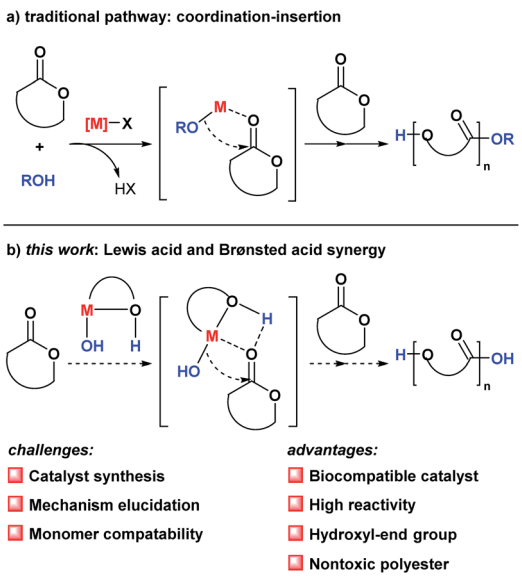

Scheme 1 Coordination–insertion mechanisms for ROP reactions: (a) metal-alkoxide catalysts; and (b) bifunctional catalysts.

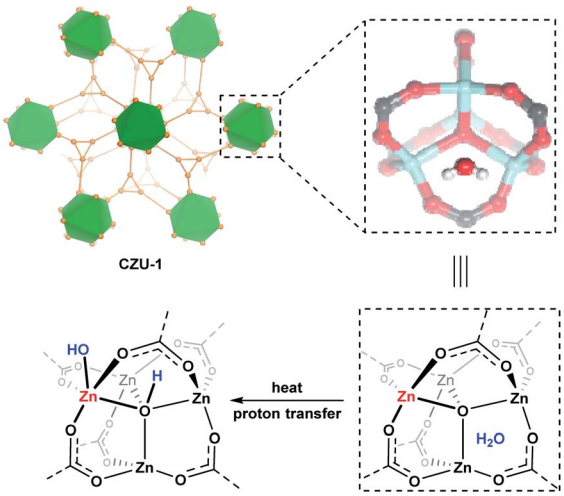

Scheme 2 Hydroxyl-based Brønsted acid generation *via* temperature-promoted proton transfer from lattice water to the oxo-bridge of CZU-1.

Results and discussion

Synthesis and characterization

CZU-1 was synthesized by heating a mixture of $Zn(OAc)_2\cdot 2H_2O$, H_2tzmb and NaOH in water at 180 °C for 3 days (see the ESI† for details). The formula of CZU-1 was established on the basis of

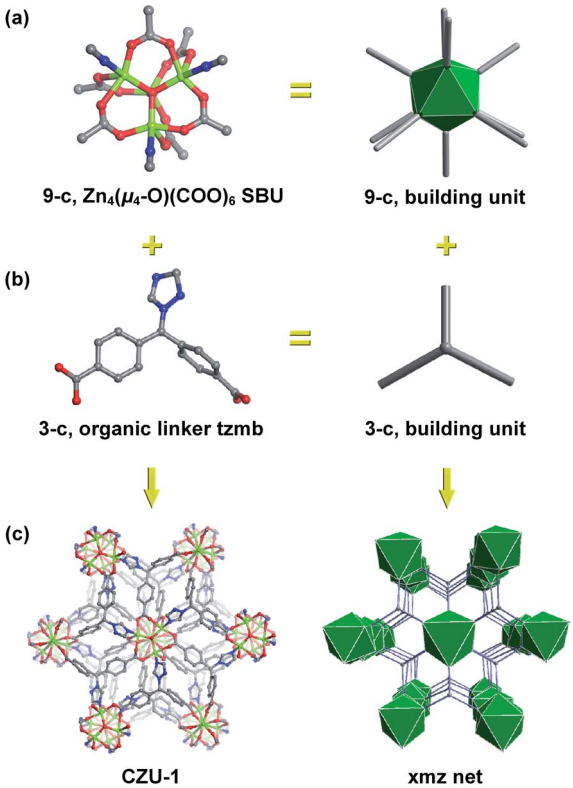

Fig. 1 The combination of 9-connected tetranuclear $Zn_4(\mu_4\text{-}O)(COO)_6$ SBUs (a) and tripodal tzmb linkers (b) results in the 3D framework of CZU-1, displaying an augmented **xmz** net (c).

single-crystal X-ray diffraction and elemental analysis studies. CZU-1 crystallizes in the trigonal $R\bar{3}$ space group, built from oxo-centered tetranuclear $Zn_4(\mu_4\text{-}O)(COO)_6$ SBUs connected by tzmb linkers (Fig. 1). The geometry of the tetranuclear $Zn_4(\mu_4\text{-}O)(COO)_6$ SBUs is similar to that observed in the IRMOF series,[14] in which four Zn^{II} atoms, coordinated to the carboxyl groups and triazole N atoms of tzmb, are connected by a μ_4-O atom. The connections between the 9-connected $Zn_4(\mu_4\text{-}O)(COO)_6$ SBUs and 3-branched tzmb result in an interesting 3D network, which can be simplified as a 3,9-connected binodal net with the point symbol $\{4^2\cdot6\}_3\{4^6\cdot6^{21}\cdot8^9\}$, corresponding to **xmz** topology.[19] It is worth noting that the lattice water molecules are involved in weak hydrogen-bonding with the carboxyl O atom ($O\cdots O_{water} = 3.465$ Å), triazole N atom ($N\cdots O_{water} = 3.760$ Å) and μ_4-O atom ($\mu_4\text{-}O\cdots O_{water} = 3.603$ Å), and should be easily activated during catalysis.

CZU-1 is thermally and chemically stable. Thermogravimetric analysis (TGA) showed that the decomposition temperature of CZU-1 is about 420 °C (Fig. S7†). Powder X-ray diffraction (PXRD) patterns showed that the robust structure of CZU-1 was retained after a crystalline sample was heated at 390 °C in air for 6 h (Fig. S8†). CZU-1 is also highly stable in various chemical environments (Fig. 2, S9 and S10†), such as being suspended in strongly acidic or basic aqueous solution (pH = 1 or 12) at room temperature, in hot water (100 °C), and in various organic solvents (DMF and DMSO) at 120 °C.

CZU-1 catalyzed solvent-free ROP reactions

The ROP reaction conditions were optimized *via* measuring the catalytic activity of CZU-1 during the bulk polymerization of L-lactide (L-LA) (Fig. S11 and S12†). When fixing the catalyst loading (0.025 mol% CZU-1), the optimized reaction temperature is 160 °C, resulting in the near-quantitative polymerization of L-LA monomers within 36 h, obtaining high molecular weight poly(L-LA) (PLLA) (up to 32 kDa) with a polydispersity index (PDI) of 1.52. Decreasing or increasing the reaction temperature leads to low molecular weight PLLA. Moreover, L-LA conversion markedly decreased when the reaction temperature was below 160 °C. At the optimized reaction temperature (160 °C), the best CZU-1 catalyst loading is 0.025 mol%. Even though the molecular weight of PLLA could be improved with lower catalyst loading, the reaction time was then markedly prolonged (60 h for 0.01 mol% CZU-1).

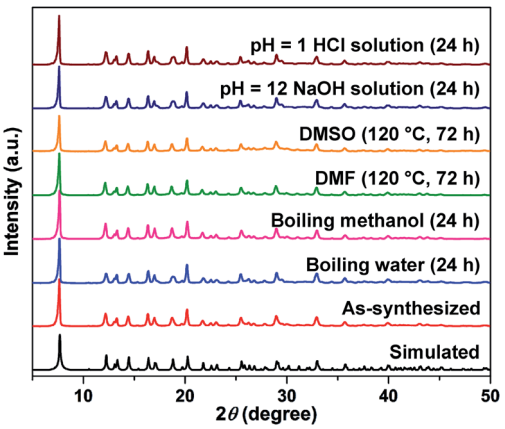

Fig. 2 PXRD patterns of as-synthesized CZU-1 and samples treated with aqueous solutions of HCl (pH = 1) and NaOH (pH = 12) for 24 h, hot DMSO and DMF solvent at 120 °C for 72 h, and boiling methanol and water for 24 h.

Considering that the lattice water in CZU-1 could not be directly removed by heating under vacuum, we used hydrated zinc salt $Zn(OAc)_2\cdot2H_2O$ and anhydrous zinc salt $Zn(OTf)_2$ as control catalysts to illustrate the roles played by water in the ROP reaction. The hydrated zinc salt $Zn(OAc)_2\cdot2H_2O$ is highly active for the bulk polymerization of L-LA (99% conversion) under identical conditions, while the anhydrous zinc salt $Zn(OTf)_2$ is inactive for the ROP reaction, indicating that water plays important roles in the ROP reaction. Compared with $Zn(OAc)_2\cdot2H_2O$, CZU-1 allows the ability to better control the molecular weight distribution (PDI = 1.52 for CZU-1 and 2.13 for $Zn(OAc)_2\cdot2H_2O$) under identical conditions; this should be ascribed to a substantial decrease in the occurrence of side transesterification reactions, which could be controlled by the bulky tetranuclear active sites present in CZU-1.

To check the stability of CZU-1, we carried out leaching and recycling experiments. When the filtrate of the reaction mixture after catalysis was used instead of CZU-1 under identical conditions, the conversion of L-LA was negligible (Fig. S14†). Inductively coupled plasma-mass spectrometry (ICP-MS) analysis showed that no zinc species leached into the supernate. These results demonstrate the heterogeneous nature of the catalyst. CZU-1 can be simply recovered *via* centrifugation and reused over successive runs while retaining the majority of its high catalytic efficiency (Fig. S15†). PXRD patterns, X-ray photoelectron spectra (XPS) and FT-IR spectra of recovered CZU-1 samples are almost identical to those of as-synthesized ones, proving the structural integrity of CZU-1 during catalysis (Fig. S16–S18†). Because the pore size of CZU-1 is very small and the molecular size of PLLA is very large, the ROP reaction should be catalyzed by the active sites on the surface of CZU-1.

Under the optimized ROP reaction conditions (160 °C and 0.025 mol% catalyst loading), as shown in Table 1, the CZU-1 catalyst exhibits good substrate compatibility with a range of cyclic mono- and diesters, as well as carbonates; these afforded the corresponding polymers with high conversions (>99%). The ROP of GA generated the PGA product with $M_n = 45.41$ kDa and PDI = 1.39 (entry 2). Unsubstituted 6-, 7-, 8- and 15-membered-ring monoesters were transformed into the corresponding products with M_n values in the range of 16.72–27.83 kDa (entries 3–6). The bulk ROPs of 4-methyl, 4,4′-dimethyl- and 6-methyl-substituted CL analogues also proceeded smoothly with complete substrate conversions (entries 7–9). Trimethylene carbonate (TMC) and its 2,2′-dimethyl-substituted analogue 2,2′-dimethyltrimethylene carbonate (DMTMC) could also be easily polymerized by the CZU-1 catalyst under identical conditions (entries 10 and 11). Having a methyl substituent at the 4- or 6-position of CL barely affected the reaction rate, but it did reduce the molecular weight of the corresponding product. A similar substituent effect was also observed for the TMC-type substrates. These results indicate that steric hindrance from different substrates could affect the polymerization degree.

Table 1 ROP of cyclic esters and carbonates catalyzed by CZU-1 in bulk[a]

Entry	Monomer	Polymer	Conv.[b] (%)	M_n[c] (kDa)	PDI
1	L-LA	PLLA	>99	32.60	1.52
2[d,f]	GA	PGA	>99	45.41	1.39
3	VL	PVL	>99	16.72	1.51
4	CL	PCL	>99	22.25	1.36
5	HL	PHL	>99	17.57	1.48
6[e,f]	PDL	PPDL	>99	27.83	1.03
7	4-MeCL	P(4-MeCL)	>99	17.23	1.43
8	4,4′-MeCL	P(4,4′-MeCL)	>99	13.80	1.59
9	6-MeCL	P(6-MeCL)	>99	11.36	1.60
10	TMC	PTMC	>99	12.74	1.62
11	DMTMC	PDMTMC	>99	8.45	1.59

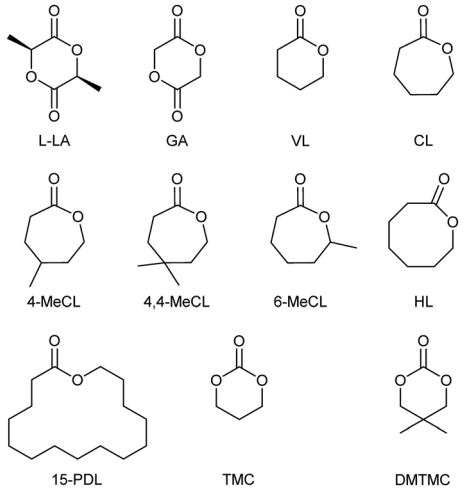

[a] Reaction conditions: [monomer] : [CZU-1] = 4000 : 1; 160 °C; 36 h. [b] Determined *via* ^{1}H NMR spectroscopy. [c] M_n and PDI were determined *via* GPC in THF in the presence of a polystyrene (PS) standard. [d] 190 °C; 36 h. [e] [Monomer] : [CZU-1] = 200 : 1; 5 days. [f] GPC in hexafluoroisopropanol (HFIP) in the presence of a poly(methyl methacrylate) (PMMA) standard.

In contrast to the well-studied solution ROP reactions involving cyclic esters catalyzed by zinc catalysts (Table S2 in the ESI†), there are few zinc-based catalysts for bulk ROP reactions reported in the literature; however, bulk polymerization is very important for practical applications, because it is organic solvent free and has minimized numbers of undesired side reactions, and large-scale production is easy.[20] Additionally, even though there are a few reported zinc complexes that are active for the bulk polymerization of L-LA, their catalytic properties are far inferior to those of CZU-1.

DFT calculations based on the CZU-1 catalyzed solvent-free ROP reaction

According to the structure of $Zn_4(\mu_4\text{-O})(COO)_6$ (Fig. S19†) in CZU-1, the direct coordination of the alkoxy oxygen of a cyclic ester (using glycolide as an example) monomer with a zinc atom is impossible because of steric hindrance. Therefore, activation of the $Zn_4(\mu_4\text{-O})(COO)_6$ cores in CZU-1 should be the first step in the catalytic ROP reaction.

The activation of $Zn_4(\mu_4\text{-O})(COO)_6$ in CZU-1. DFT calculations (see ESI† for details) revealed that the guest water molecules in CZU-1 weakly interact with $Zn_4(\mu_4\text{-O})(COO)_6$ (Fig. 3). Under the optimized catalytic conditions, one water hydrogen was transferred to the μ_4-O atom of $Zn_4(\mu_4\text{-O})(COO)_6$, generating a μ_4-OH Brønsted acid site. The remaining hydroxyl group of water coordinates to one Zn atom as a nucleophilic attack center. The calculated activation energy barrier of this process is 28.8 kcal mol^{-1}.

Initiation. The initiation of the ROP reaction involves forming the precursor complex **2a** between the monomer and activated catalytic center (Fig. 4). The binding pattern of this complex involves strong hydrogen bonding between μ_4-OH and the carbonyl oxygen of glycolide (H-bond length of 1.843 Å), weak hydrogen bonding between Zn–OH and H–C on the glycolide ring (2.201 and 2.349 Å), and a weak interaction between the carbonyl oxygen and hydroxylated Zn atom (3.317 Å). The binding energy for the formation of this complex is 25.5 kcal mol^{-1}. This high binding energy indicates that the activated $Zn_4(\mu_4\text{-O})(COO)_6$ core can readily capture a monomer to initiate the ROP reaction.

The hydroxyl group at the activated $Zn_4(\mu_4\text{-O})(COO)_6$ core can undergo the nucleophilic attack of the carbonyl group of glycolide, resulting in the formation of a new C–O bond between glycolide and the hydroxyl group. Meanwhile, the carbonyl C=O π-bond of the monomer is broken *via* the four-membered-ring transition state **2aTS**. The corresponding activation energy barrier is 11.7 kcal mol^{-1}, which is much lower than that for the activation of the $Zn_4(\mu_4\text{-O})(COO)_6$ cluster unit. The shortened μ_4-OH···O H-bond (1.808 Å in **2aTS** *vs.* 1.843 Å in **2a**) indicates the importance of μ_4-OH in this elementary reaction step.

This elementary step leads to the transformation of the carbonyl C=O double bond into a C–O single bond in the intermediate product (**2b**) *via* a bifurcated bonding pattern. The carbonyl C adopts an sp^3 bonding pattern in **2b**, which is favorable for the formation of a ring-opening intermediate (**2c**) *via* rotating the C–O bond to relocate the acyl oxygen atom. The low activation energy barrier of the transition state (**2bTS**) (4.4 kcal mol^{-1}) indicates that the corresponding C–O single bond is easily rotated. In the subsequent ring rupture step, the

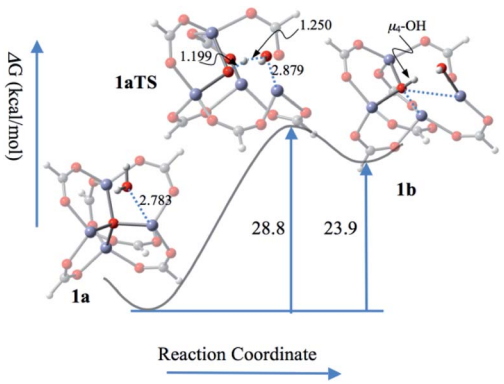

Fig. 3 The reaction profile of the water-activation process of $Zn_4(\mu_4\text{-O})(COO)_6$ from CZU-1. Color scheme: O, red; H, light grey; C, gray; Zn, blue.

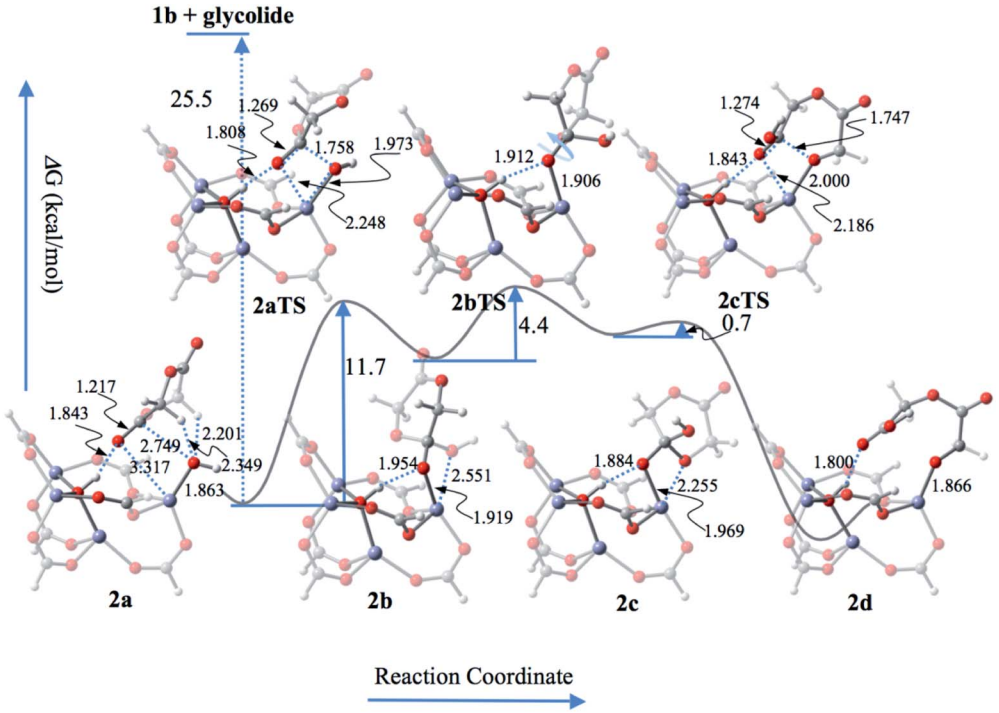

Fig. 4 The reaction profile of the initiation of the ROP reaction catalyzed by $Zn_4(\mu_4\text{-}O)(COO)_6$ from CZU-1. Color scheme: O, red; H, light grey; C, gray; Zn, blue.

activation energy barrier (0.7 kcal mol^{-1}) is much lower than that for the transformation from a carbonyl C=O double bond to a C–O single bond (**2aTS**, 11.7 kcal mol^{-1}). This process is accompanied by the formation of a new carbonyl C=O double bond in the transition state **2cTS** and the ring ruptured product **2d.** The initiation step is then completed through the formation of the ring-opened monomer–catalyst complex **2d.**

Propagation. Fig. 5 summarizes the propagation pathway of the ROP reaction catalyzed by CZU-1. The propagation of the ROP reaction follows the initiation pathway, except that the Zn–OH group in the initiation stage is replaced by Zn–OR, in which R represents the glycolide polymer segment. A methyl group has been applied to mimic the R group in the present computational study. In the propagation stage, the activation energy for

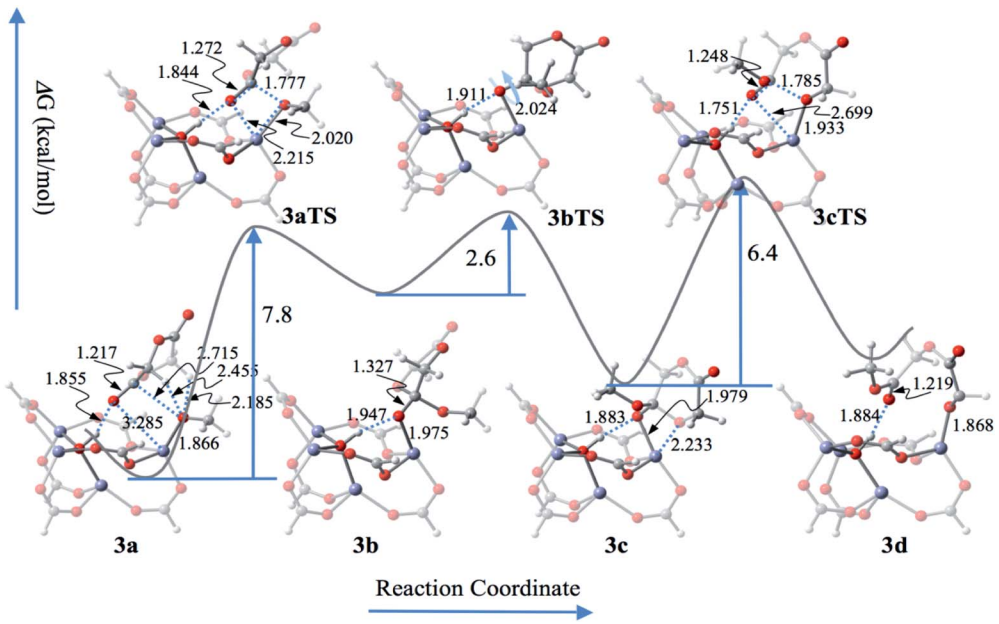

Fig. 5 The reaction profile of the ROP propagation process catalyzed by $Zn_4(\mu_4\text{-}O)(COO)_6$. Color scheme: O, red; H, light grey; C, gray; Zn, blue.

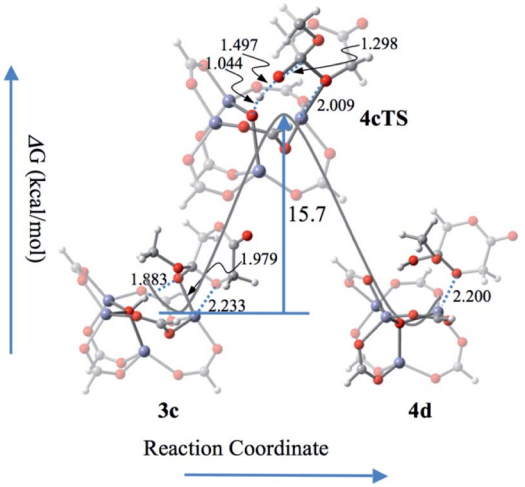

Fig. 6 The reaction profile of the deprotonation of μ_4-OH for the termination of the ROP reaction process. Color scheme: O, red; H, light grey; C, gray; Zn, blue.

the OR nucleophilic attack of the glycolide carbonyl group is computed to be 7.8 kcal mol^{-1}, which is about 4 kcal mol^{-1} lower than the related step in the initiation process. On the other hand, the activation energy barrier for breaking the ringed acyl C–O bond is 6.3 kcal mol^{-1}, which is about 5.5 kcal mol^{-1} higher than the corresponding initiation step.

Termination. The deprotonation of μ_4-OH is the main factor for the termination of the ROP process catalyzed by CZU-1. As shown in Fig. 6, **3c** is found to be the most probable intermediate for the deprotonation of μ_4-OH, and **4cTS** is the corresponding transition state. The activation energy barrier for the deprotonation process is 15.7 kcal mol^{-1}.

According to the coordination–insertion polymerization mechanism, the molecular-weight is controlled by the ratios $k_{propagation}/k_{initiation}$ and $k_{propagation}/k_{termination}$.[1] Based on the present mechanism, the molecular weight should be evaluated according to either the ratio $\exp(-G_{3aTS}/RT)/\exp(-G_{1aTS}/RT)$ for the former or the ratio $\exp(-G_{4cTS}/RT)/\exp(-G_{3cTS}/RT)$ for the latter.

It is worth noting that the carbonyl oxygen atom of glycolide undergoes strong hydrogen bonding with μ_4-OH in all reaction steps, including the initiation and propagation processes, which is similar to the mechanisms proposed for guanidine triazabicyclodecene,[21] thiomidate,[2g] and other proton shuttle catalysts.[22] In other words, the Brønsted acid center μ_4-OH in activated $Zn_4(\mu_4\text{-}O)(COO)_6$ plays key roles in the catalytic ROP reaction.

On the basis of the above computational studies, a novel reaction pathway for the CZU-1 catalyzed ROP process is proposed, which includes activation, initiation, propagation, and termination processes (Scheme 3). First, proton transfer from a guest water molecule to the oxo bridge of the $Zn_4(\mu_4\text{-}O)(COO)_6$-based cluster leads to a hydroxo-bridged intermediate **I**, creating a Brønsted acid μ_4-OH moiety. Second, an unprecedented ROP initiation model **II**, based upon the synergy of the Lewis acid Zn(II)–OH site and Brønsted acid μ_4-OH, was obtained. Then, the nucleophilic attack of the carbonyl group by the hydroxyl group of the activated Zn(II)–OH site generates the intermediate **III**, which then undergoes ring-opening to afford the intermediate **V**. Further chain propagation proceeds through the synergistic initiation cycle. Finally, the termination of the growing chain, caused by the deprotonation of μ_4-OH, results in the formation of the polyester product **VI** with hydroxyl end groups. The rate controlling step of this reaction pathway is the activation step, with an activation energy of 28.8 kcal mol^{-1}. This reaction is unlikely to take place at room temperature. When heated to 160 °C, the rate of this step is estimated to be 0.014 s^{-1}, indicating that an observable reaction should thus be expected.

Experimental verification of the proposed mechanism for the ROP reaction

According to the mechanism proposed above, the activation process consists of proton transfer from water to μ_4-O in $Zn_4(\mu_4$-

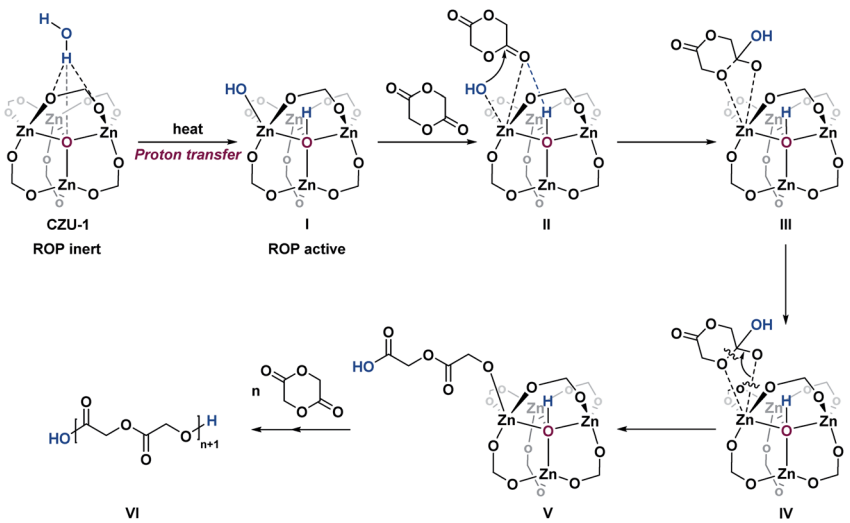

Scheme 3 The proposed mechanism for the CZU-1 catalyzed ring-opening polymerization of glycolide.

O)(COO)$_6$, generating a Brønsted acid center, μ_4-OH, to initiate the ROP reaction. To verify this prediction, temperature-dependent IR spectra of CZU-1 were collected *via in situ* diffuse reflectance infrared Fourier transform spectroscopy (DRIFTS). The broad peaks centered at 3510 and 3645 cm^{-1} (the O–H stretching vibrations of lattice water) shift to 3560 and 3675 cm^{-1}, respectively, when the temperature is raised to 130 °C (Fig. 7). The peak centered at 3560 cm^{-1} corresponds to the O–H stretching vibration of μ_4-OH.[23] It is worth noting that the temperature-dependent proton transfer process from guest water to the oxo-bridge of CZU-1 is irreversible (Fig. 7, inset), which is favorable for the ROP reaction.

DFT calculations predicted that the polyester products feature hydroxyl end groups that are controlled by the initiating μ_4-OH group. To determine the terminal end groups of the resulting polymer, we performed MALDI-TOF MS experiments on the PCL product. MALDI-TOF MS showed a single distribution of a series of peaks at $114n + 18 + 23$ with a charge of +1, which can be assigned to n(CL) + H_2O + Na^+ (Fig. 8). This result confirmed the presence of hydroxyl end groups in the resultant polyester chains, which is consistent with the μ_4-OH moieties acting as initiating groups, thus supporting the proposed mechanism obtained *via* DFT calculations.

Toxicity tests

Fibroblasts (FBs) are a type of cell involved in the synthesis of extracellular matrices and collagen, the structural frameworks of human and animal tissues and connective tissues, which play a critical role in wound healing. Smooth muscle cells (SMCs), known as myocytes, grow around blood vessels, bronchia, the stomach and the bladder to control starch. Both types of cells are commonly involved in wound healing after clinical surgery and come into close contact with artificial biomaterials, such as the surgical sutures used in surgery. In this work, three pairs of

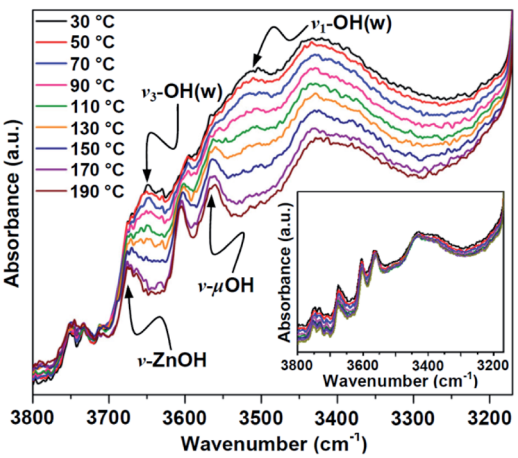

Fig. 7 Temperature-dependent *in situ* DRIFT spectra of as-prepared CZU-1 labeled with the changes in the stretching vibrations of the hydroxyl groups from 30 to 190 °C under a dry Ar atmosphere (the inset shows DRIFT spectra of activated CZU-1 samples showing the changes in the stretching vibrations of the hydroxyl groups upon decreasing the temperature from 190 to 50 °C).

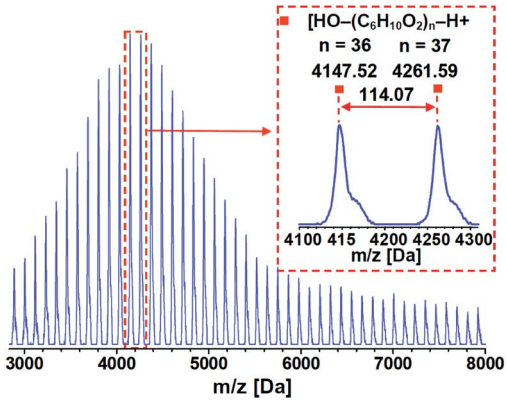

Fig. 8 MALDI-TOF MS from a PCL sample (88% conversion, M_n = 12.6 kDa and PDI = 1.06) prepared *via* the ROP of CL with [CZU-1] : [CL] = 1 : 500.

different polyesters [PLLA-CZU-1/PLLA-Sn(Oct)$_2$, PGA-CZU-1/PGA-Sn(Oct)$_2$, and PCL-CZU-1/PCL-Sn(Oct)$_2$], containing equimolar quantities of Zn or Sn, were prepared *via* the bulk ROP of cyclic esters (L-LA, GA, and CL) using CZU-1 and Sn(Oct)$_2$ catalysts, respectively. We further conducted a series of FB- and SMC-based cytotoxicity studies on the catalysts and polyesters

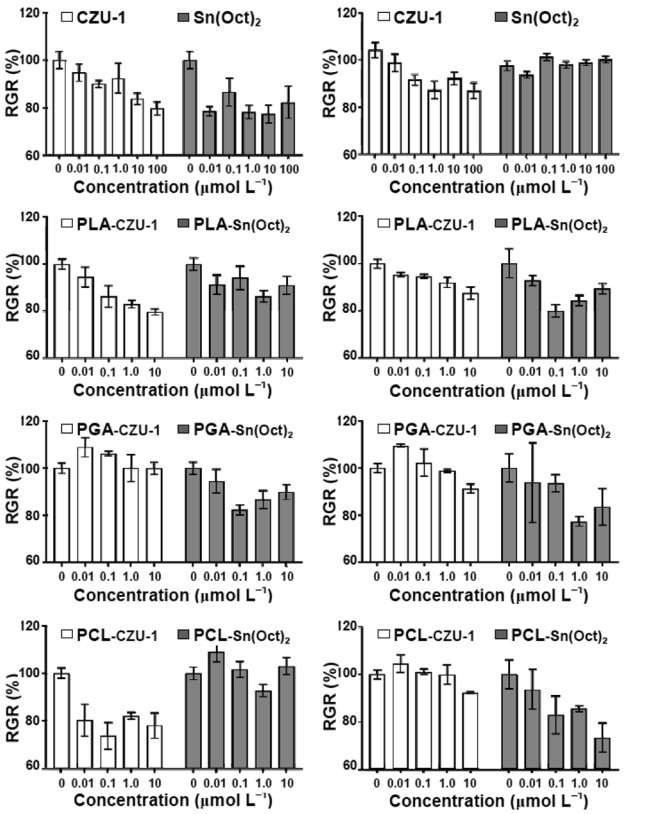

Fig. 9 The effects of CZU-1, PLLA-CZU-1, PGA-CZU-1 and PCL-CZU-1 (white), and Sn(Oct)$_2$, PLLA-Sn(Oct)$_2$, PGA-Sn(Oct)$_2$ and PCL-Sn(Oct)$_2$ (dark) at different Zn or Sn concentrations (0, 0.01, 0.1, 1.0, 10, and 100 μmol L^{-1}), respectively, on the relative growth rates (RGRs) of fibroblasts (left column) and smooth muscle cells (right column); mean ± SEM, n = 6.

to investigate possible toxicity effects on these two types of cells, and compared PLLA, PGA and PCL with and without Sn.

As shown in Fig. 9, the data from toxicity studies for these six polyester materials demonstrated that, up to 10 μmol L^{-1}, PGA-CZU-1 did not affect the growth rates of both cell types, while PLLA-CZU-1, PCL-CZU-1 and CZU-1 showed dose-dependent effects on FBs. Toward SMCs, PLLA-CZU-1, PCL-$Sn(Oct)_2$ and CZU-1 affected cell growth dose-dependently. Compared with $Sn(Oct)_2$, CZU-1 generated better outcomes for FBs, and there was not much difference in the case of SMCs. Interestingly, the data from this study reveals that the RGR% values of some polyester materials are above those of untreated control cells (100%), indicating that these polyester materials did not affect cell growth, which is good for keeping tissue intact. Among these six materials, PCL-CZU-1 showed strong non-toxic potential, generating the possibility that it could be used in medical artificial biomaterials for ophthalmology, drug delivery systems, surgical mending, bone fixing and tissue repair.

Conclusions

In summary, we demonstrated for the first time the solvent-free ROP of cyclic esters catalyzed using a biocompatible coordination network, CZU-1, consisting of oxo/hydroxo-bridged $Zn_4(\mu_4\text{-}O)(COO)_6$ SBUs and guest water; this showed great potential for the ROP synthesis of biocompatible polyesters. DFT calculations revealed that the guest water in CZU-1 played crucial roles in the key steps of the ROP reactions by generating active Brønsted acid μ_4-OH and Lewis acid Zn–OH sites *via* proton transfer from water to μ_4-O in the $Zn_4(\mu_4\text{-}O)(COO)_6$ SBU, which is different to mechanisms reported in the literature for solvent-free ROP reactions. The mechanistic research results highlight the potential of combining Brønsted and Lewis acid sites in ROP catalysts to synergistically improve the catalytic efficiency. Temperature-dependent *in situ* DRIFTS experiments confirmed the presence of an irreversible intermolecular proton transformation process. DFT calculation and MALDI-TOF MS analysis results showed that the resulting polyester chains feature hydroxyl end groups, which can be readily post-modified for biomedical applications. We hope that this newly developed mechanism will stimulate extensive research into biocompatible ROP catalysts for the solvent-free ROP of cyclic esters, generating biocompatible polyesters for biomedical applications.

Abbreviations

ROP	Ring-opening polymerization
MOFs	Metal–organic frameworks
SBUs	Secondary building units
Tzmb	4,4′-(1*H*-1,2,4-Triazol-1-yl)methylene-bis(benzoate)
DMF	*N*,*N*′-Dimethylformamide
DMSO	Dimethylsulfoxide
THF	Tetrahydrofuran
HFIP	Hexafluoroisopropanol
L-LA	L-Lactide
GA	Glycolide
VL	δ-Valerolactone
CL	ε-Caprolactone
4-MeCL	4-Methyl-ε-caprolactone
4,4-MeCL	4,4-Dimethyl-ε-caprolactone
6-MeCL	6-Methyl-ε-caprolactone
HL	7-Heptalactone
PDL	15-Pentadecalactone
TMC	Trimethylene carbonate
DMTMC	2,2-Dimethyltrimethylene carbonate
PLLA	Poly(L-lactide)
PGA	Polyglycolide
PVL	Poly(δ-valerolactone)
PCL	Poly(ε-caprolactone)
PHL	Poly(7-heptalactone)
PPDL	Poly(15-pentadecalactone)
P(4-MeCL)	Poly(4-methyl-ε-caprolactone)
P(4,4′-MeCL)	Poly(4,4′-dimethyl-ε-caprolactone)
P(6-MeCL)	Poly(6-methyl-ε-caprolactone)
PTMC	Poly(trimethylene carbonate)
PDMTMC	Poly(2,2-dimethyltrimethylene carbonate)
PMMA	Poly(methyl methacrylate)
PS	Polystyrene
GPC	Gel-permeation chromatography
M_n	Number average molecular weight
M_w	Weight average molecular weight
PDI	Polydispersity index
FBs	Fibroblasts
SMCs	Smooth muscle cells
FCS	Fetal calf serum
DRs	Dissolution rates
SEM	Standard error of mean
RGR	Relative growth rate
DFT	Density functional theory
DRIFTS	Diffuse reflectance IR Fourier transform spectroscopy
MALDI-TOF MS	Matrix-assisted laser desorption/ionization time-of-flight mass spectroscopy
HRMS	High resolution mass spectroscopy
FT-IR	Fourier transform infrared
TGA	Thermogravimetric analysis
PXRD	Powder X-ray diffraction
ICP-MS	Inductively coupled plasma-mass spectrometry
XPS	X-ray photoelectron spectroscopy

Conflicts of interest

There are no conflicts to declare.

Acknowledgements

This research was supported by the National Natural Science Foundation of China (21676030, 11775037 and 21872122), a Project Funded by the Priority Academic Program Development of Jiangsu Higher Education Institutions, the Advanced

Catalytic and Green Manufacturing Collaborative Innovation Center, Changzhou University and Jiangsu Key Laboratory of Advanced Catalytic Materials and Technology (ZZZD201807 and BM2012110).

Notes and references

1 (*a*) O. Dechy-Cabaret, B. Martin-Vaca and D. Bourissou, *Chem. Rev.*, 2004, **104**, 6147–6176; (*b*) M. Labet and W. Thielemans, *Chem. Soc. Rev.*, 2009, **38**, 3484–3504; (*c*) M. J. Stanford and A. P. Dove, *Chem. Soc. Rev.*, 2010, **39**, 486–494; (*d*) C. M. Thomas, *Chem. Soc. Rev.*, 2010, **39**, 165–173; (*e*) A. Tardy, J. Nicolas, D. Gigmes, C. Lefay and Y. Guillaneuf, *Chem. Rev.*, 2017, **117**, 1319–1406; (*f*) G. Becker and F. R. Wurm, *Chem. Soc. Rev.*, 2018, **47**, 7739–7782.

2 (*a*) A. K. Sutar, T. Maharana, S. Dutta, C.-T. Chen and C.-C. Lin, *Chem. Soc. Rev.*, 2010, **39**, 1724–1746; (*b*) S. Dagorne, M. Normand, E. Kirillov and J.-F. Carpentier, *Coord. Chem. Rev.*, 2013, **257**, 1869–1886; (*c*) Y. Sarazin and J.-F. Carpentier, *Chem. Rev.*, 2015, **115**, 3564–3614; (*d*) A. B. Kremer and P. Mehrkhodavandi, *Coord. Chem. Rev.*, 2019, **380**, 35–57; (*e*) D. M. Lyubov, A. O. Tolpygin and A. A. Trifonov, *Coord. Chem. Rev.*, 2019, **392**, 83–145; (*f*) S. Naumann, P. B. V. Scholten, J. A. Wilson and A. P. Dove, *J. Am. Chem. Soc.*, 2015, **137**, 14439–14445; (*g*) X. Zhang, G. O. Jones, J. L. Hedrick and R. M. Waymouth, *Nat. Chem.*, 2016, **8**, 1047–1053; (*h*) B. Lin and R. M. Waymouth, *J. Am. Chem. Soc.*, 2017, **139**, 1645–1652; (*i*) T. Stoesser and C. K. Williams, *Angew. Chem., Int. Ed.*, 2018, **57**, 6337–6341.

3 H. R. Kricheldorf, I. Kreiser-Saunders and A. Stricker, *Macromolecules*, 2000, **33**, 702–709.

4 T. M. Ovitt and G. W. Coates, *J. Am. Chem. Soc.*, 1999, **121**, 4072–4073.

5 (*a*) W. M. Stevels, M. J. K. Ankoné, P. J. Dijkstra and J. Feijen, *Macromolecules*, 1996, **29**, 3332–3333; (*b*) X. Wang, J. L. Brosmer, A. Thevenon and P. L. Diaconescu, *Organometallics*, 2015, **34**, 4700–4706.

6 (*a*) V. Simic, N. Spassky and L. G. Hubert-Pfalzgraf, *Macromolecules*, 1997, **30**, 7338–7340; (*b*) E. Martin, P. Dubois and R. Jerome, *Macromolecules*, 2000, **33**, 1530–1535; (*c*) B. J. O'Keefe, S. M. Monnier, M. A. Hillmyer and W. B. Tolman, *J. Am. Chem. Soc.*, 2001, **123**, 339–340.

7 (*a*) R. H. Platel, L. M. Hodgson and C. K. Williams, *Polym. Rev.*, 2008, **48**, 11–63; (*b*) E. Piedra-Arroni, C. Ladavière, A. Amgoune and D. Bourissou, *J. Am. Chem. Soc.*, 2013, **135**, 13306–13309; (*c*) D. S. Bolotin, V. Korzhikov-Vlakh, E. Sinitsyna, S. N. Yunusova, V. V. Suslonov, A. Shetnev, A. Osipyan, M. Krasavin and V. Y. Kukushkin, *J. Catal.*, 2019, **372**, 362–369.

8 (*a*) P. Dubois, N. Ropson, R. Jerome and P. Teyssie, *Macromolecules*, 1996, **29**, 1965–1975; (*b*) N. Nomura, R. Ishii, M. Akakura and K. Aoi, *J. Am. Chem. Soc.*, 2002, **124**, 5938–5939; (*c*) L. R. Rieth, D. R. Moore, E. B. Lobkovsky and G. W. Coates, *J. Am. Chem. Soc.*, 2002, **124**, 15239–15248; (*d*) I. Yu, A. Acosta-Ramirez and P. Mehrkhodavandi, *J. Am. Chem. Soc.*, 2012, **134**, 12758–12773; (*e*) R. Ligny, M. M. Hänninen, S. M. Guillaume and J.-F. Carpentier, *Angew. Chem., Int. Ed.*, 2017, **56**, 10388–10393.

9 (*a*) M. Ryner, K. Stridsberg, A.-C. Albertsson, H. von Schenck and M. Svensson, *Macromolecules*, 2001, **34**, 3877–3881; (*b*) E. L. Marshall, V. C. Gibson and H. S. Rzepa, *J. Am. Chem. Soc.*, 2005, **127**, 6048–6051; (*c*) Y. Sarazin, B. Liu, T. Roisnel, L. Maron and J.-F. Carpentier, *J. Am. Chem. Soc.*, 2011, **133**, 9069–9087; (*d*) C. Robert, T. E. Schmid, V. Richard, P. Haquette, S. K. Raman, M.-N. Rager, R. M. Gauvin, Y. Morin, X. Trivelli, V. Guérineau, I. del Rosal, L. Maron and C. M. Thomas, *J. Am. Chem. Soc.*, 2017, **139**, 6217–6225.

10 W. Dittrich and R. C. Schulz, *Angew. Makromol. Chem.*, 1971, **15**, 109–126.

11 (*a*) H. von Schenck, M. Ryner, A.-C. Albertsson and M. Svensson, *Macromolecules*, 2002, **35**, 1556–1562; (*b*) J. L. Eguiburu, M. J. Fernandez-Berridi, F. P. Cossío and J. S. Román, *Macromolecules*, 1999, **32**, 8252–8258.

12 (*a*) O. M. Yaghi, M. O'Keeffe, N. W. Ockwig, H. K. Chae, M. Eddaoudi and J. Kim, *Nature*, 2003, **423**, 705–714; (*b*) J. Y. Lee, O. K. Farha, J. Roberts, K. A. Scheidt, S. B. T. Nguyen and J. T. Hupp, *Chem. Soc. Rev.*, 2009, **38**, 1450–1459; (*c*) L. Ma, C. Abney and W. Lin, *Chem. Soc. Rev.*, 2009, **38**, 1248–1256; (*d*) J.-R. Li, R. J. Kuppler and H.-C. Zhou, *Chem. Soc. Rev.*, 2009, **38**, 1477–1504; (*e*) H. Furukawa, K. E. Cordova, M. O'Keeffe and O. M. Yaghi, *Science*, 2013, **341**, 974; (*f*) Q.-L. Zhu and Q. Xu, *Chem. Soc. Rev.*, 2014, **43**, 5468–5512; (*g*) A. Schoedel, M. Li, D. Li, M. O'Keeffe and O. M. Yaghi, *Chem. Rev.*, 2016, **116**, 12466–12535; (*h*) W. P. Lustig, S. Mukherjee, N. D. Rudd, A. V. Desai, J. Li and S. K. Ghosh, *Chem. Soc. Rev.*, 2017, **46**, 3242–3285.

13 (*a*) C. Serre, F. Millange, S. Surblé and G. Férey, *Angew. Chem., Int. Ed.*, 2004, **43**, 6286–6289; (*b*) P. Horcajada, C. Serre, M. Vallet-Regí, M. Sebban, F. Taulelle and G. Férey, *Angew. Chem., Int. Ed.*, 2006, **45**, 5974–5978; (*c*) L. Hamon, C. Serre, T. Devic, T. Loiseau, F. Millange, G. Férey and G. De Weireld, *J. Am. Chem. Soc.*, 2009, **131**, 8775–8777.

14 (*a*) H. Li, M. Eddaoudi, M. O'Keeffe and O. M. Yaghi, *Nature*, 1999, **402**, 276–279; (*b*) M. Eddaoudi, J. Kim, N. Rosi, D. Vodak, J. Wachter, M. O'Keeffe and O. M. Yaghi, *Science*, 2002, **295**, 469–472; (*c*) A. R. Millward and O. M. Yaghi, *J. Am. Chem. Soc.*, 2005, **127**, 17998–17999; (*d*) H. Deng, C. J. Doonan, H. Furukawa, R. B. Ferreira, J. Towne, C. B. Knobler, B. Wang and O. M. Yaghi, *Science*, 2010, **327**, 846–850.

15 K. Koh, A. G. Wong-Foy and A. J. Matzger, *Angew. Chem., Int. Ed.*, 2008, **47**, 677–680.

16 (*a*) M. Kandiah, M. H. Nilsen, S. Usseglio, S. Jakobsen, U. Olsbye, M. Tilset, C. Larabi, E. A. Quadrelli, F. Bonino and K. P. Lillerud, *Chem. Mater.*, 2010, **22**, 6632–6640; (*b*) H. Fei, J. Shin, Y. S. Meng, M. Adelhardt, J. Sutter, K. Meyer and S. M. Cohen, *J. Am. Chem. Soc.*, 2014, **136**, 4965–4973; (*c*) B. An, J. Zhang, K. Cheng, P. Ji, C. Wang and W. Lin, *J. Am. Chem. Soc.*, 2017, **139**, 3834–3840; (*d*)

X.-P. Wu, L. Gagliardi and D. G. Truhlar, *J. Am. Chem. Soc.*, 2018, **140**, 7904–7912.

17 (*a*) Y. Liu, J. F. Eubank, A. J. Cairns, J. Eckert, V. C. Kravtsov, R. Luebke and M. Eddaoudi, *Angew. Chem., Int. Ed.*, 2007, **46**, 3278–3283; (*b*) S.-T. Zheng, T. Wu, F. Zuo, C. Chou, P. Feng and X. Bu, *J. Am. Chem. Soc.*, 2012, **134**, 1934–1937; (*c*) K. Wang, D. Feng, T.-F. Liu, J. Su, S. Yuan, Y.-P. Chen, M. Bosch, X. Zou and H.-C. Zhou, *J. Am. Chem. Soc.*, 2014, **136**, 13983–13986; (*d*) T. Ikuno, J. Zheng, A. Vjunov, M. Sanchez-Sanchez, M. A. Ortuño, J. L. Fulton, D. M. Camaioni, Z. Li, D. Ray, B. L. Mehdi, N. D. Browning, O. K. Farha, J. T. Hupp, C. J. Cramer, L. Gagliardi and J. A. Lercher, *J. Am. Chem. Soc.*, 2017, **139**, 10294–10301; (*e*) P. Ji, K. Manna, Z. Lin, X. Feng, A. Urban, Y. Song and W. Lin, *J. Am. Chem. Soc.*, 2017, **139**, 7004–7011; (*f*) Y. Keum, S. Park, Y.-P. Chen and J. Park, *Angew. Chem., Int. Ed.*, 2018, **57**, 14852–14856.

18 (*a*) C.-Y. Sun, S.-X. Liu, D.-D. Liang, K.-Z. Shao, Y.-H. Ren and Z.-M. Su, *J. Am. Chem. Soc.*, 2009, **131**, 1883–1888; (*b*) R. Srirambalaji, S. Hong, R. Natarajan, M. Yoon, R. Hota, Y. Kim, Y. H. Ko and K. Kim, *Chem. Commun.*, 2012, **48**, 11650–11652; (*c*) J. Jiang and O. M. Yaghi, *Chem. Rev.*, 2015, **115**, 6966–6997; (*d*) B. Li, K. Leng, Y. Zhang, J. J. Dynes, J. Wang, Y. Hu, D. Ma, Z. Shi, L. Zhu, D. Zhang, Y. Sun, M. Chrzanowski and S. Ma, *J. Am. Chem. Soc.*, 2015, **137**, 4243–4248; (*e*) W.-Y. Gao, H. Wu, K. Leng, Y. Sun and S. Ma, *Angew. Chem., Int. Ed.*, 2016, **55**, 5472–5476; (*f*) Y.-B. Huang, J. Liang, X.-S. Wang and R. Cao, *Chem. Soc. Rev.*, 2017, **46**, 126–157; (*g*) C. A. Trickett, T. M. Osborn Popp, J. Su, C. Yan, J. Weisberg, A. Huq, P. Urban, J. Jiang, M. J. Kalmutzki, Q. Liu, J. Baek, M. P. Head-Gordon, G. A. Somorjai, J. A. Reimer and O. M. Yaghi, *Nat. Chem.*, 2019, **11**, 170–176; (*h*) W. Gong, X. Chen, H. Jiang, D. Chu, Y. Cui and Y. Liu, *J. Am. Chem. Soc.*, 2019, **141**, 7498–7508; (*i*) P. Liu, E. Redekop, X. Gao, W.-C. Liu, U. Olsbye and G. A. Somorjai, *J. Am. Chem. Soc.*, 2019, **141**, 11557–11564.

19 J. Jia X. Lin, C. Wilson, A. J. Blake, N. R. Champness, P. Hubberstey, G. Walker, E. J. Cussen and M. Schröder, *Chem. Commun.*, 2007, **8**, 840–842.

20 (*a*) J. Börner, U. Flörke, K. Huber, A. Döring, D. Kuchling and S. Herres-Pawlis, *Chem. – Eur. J.*, 2009, **15**, 2362–2376; (*b*) Q. Shi, J. Yang and X. Lü, *Inorg. Chem. Commun.*, 2015, **59**, 61–62.

21 A. Chuma, H. W. Horn, W. C. Swope, R. C. Pratt, L. Zhang, B. G. Lohmeijer, C. G. Wade, R. M. Waymouth, J. L. Hedrick and J. E. Rice, *J. Am. Chem. Soc.*, 2008, **130**, 6749–6754.

22 N. Susperregui, D. Delcroix, B. Martin-Vaca, D. Bourissou and L. Maron, *J. Org. Chem.*, 2010, **75**, 6581–6587.

23 D. Armentano, G. D. Munno, T. F. Mastropietro, M. Julve and F. Lloret, *J. Am. Chem. Soc.*, 2005, **127**, 10778–10779.

